ADVANCED ENERGY MATERIALS
www.advenergymat.de

Halogenated Polycyclic Aromatic Hydrocarbon for Hole Selective Layer/Perovskite Interface Modification and Passivation for Efficient Perovskite-Organic Tandem Solar Cells with Record Fill Factor

Md Arafat Mahmud, Jianghui Zheng, Jia-Fu Chang, Guoliang Wang, Chwenhaw Liao, Md Habibur Rahman, Walia Binte Tarique, Shi Tang, Jueming Bing, Christopher G. Bailey, Zhuofeng Li, Limei Yang, Nina Novikova, Tik Lun Leung, Hongjun Chen, Jianpeng Yi, Runmin Tao, Marko Jankovec, Stephen P. Bremner, Julie Cairney, Ashraf Uddin, Hieu T. Nguyen, Trevor Smith, Chu-Chen Chueh, and Anita W. Y. Ho-Baillie**

Perovskite whentandemed with organic photovoltaics (OPV) for double-junctions have efficiencypotentials over 40%. However, there is still room for improvement suchas better current matching, higher fill factor, as well as lower voltage and fill factor losses in the top perovskite cell. Here weaddress the issue associated with the top perovskite cell by utilising anovel halogenated polycyclic aromatic hydrocarbon compound, 1-naphthylammoniumchloride (NA—Cl) playing dual roles of surface modification for the hole selectivelayer (HSL) and passivation of HSL/perovskiteinterface. Results of X-ray photoelectron spectroscopy and density functionaltheory calculations reveal that NA—Cl retains self-assembly property for the HSLwhile demonstrating high dipole moment and polarizability. This induces asurface dipole at the HSL/perovskite interface reducing the energetic barrierfor hole extraction by 210 meV thereby enhancing voltage output and fill factorof the device. Such scheme when implemented in a high bandgap (1.78 eV)perovskite solar cell, results in a respectable efficiency of 19.7% and thehighest fill factor of 85.4% amongst those of 1.78 eV perovskite cells reported.We have also achieved 23% cell efficient monolithic perovskite-OPV tandem withan impressive fill factor of 84%, which is the highest for perovskite-OPVtandem cells reported to-date.

1. Introduction

Next-generation solar cell based on metal-halide perovskite solar cell is the fastest-growing photovoltaic technology in terms of efficiency improvement. The best laboratory cell efficiency has reached 26.7% (certified) in 2024[1] from 3.8% (in-house measured) when the first cell was reported in 2009.[2] The full advantages of perovskite solar cells, such as their bandgap-tunability, can be further utilized when they are implemented in tandems, which have higher efficiency potentials (≈45% for double junctions and ≈51% for triple-junctions) than single-junctions (≈33%).[3] While perovskite-Si tandems have the highest number of demonstrations reported,[3] the Si bottom cells in these demonstrations are in bulk-wafer-form which are rigid, making it difficult, although not impossible, for

M. A. Mahmud, J. Zheng, G. Wang, C. Liao, S. Tang, J. Bing, C. G. Bailey, T. L. Leung, H. Chen, J. Yi, R. Tao, A. W. Y. Ho-Baillie
School of Physics
The University of Sydney
Sydney, NSW 2006, Australia
E-mail: md.mahmud@sydney.edu.au; anita.ho-baillie@sydney.edu.au

M. A. Mahmud, J. Zheng, G. Wang, C. Liao, S. Tang, J. Bing, C. G. Bailey, T. L. Leung, H. Chen, J. Yi, R. Tao, A. W. Y. Ho-Baillie
The University of Sydney Nano Institute (Sydney Nano)
The University of Sydney
Sydney, NSW 2006, Australia

J. Zheng, M. H. Rahman, W. B. Tarique, S. P. Bremner, A. Uddin, A. W. Y. Ho-Baillie
Australian Centre for Advanced Photovoltaics (ACAP)
School of Photovoltaic and Renewable Energy Engineering
University of New South Wales
Sydney 2052, Australia

J. Zheng
Sustainable Energy Research Centre
School of Engineering
Macquarie University
Sydney, NSW 2109, Australia

J.-F. Chang, C.-C. Chueh
Department of Chemical Engineering
National Taiwan University, Taiwan

The ORCID identification number(s) for the author(s) of this article can be found under https://doi.org/10.1002/aenm.202400691

DOI: 10.1002/aenm.202400691

flexible applications. Perovskite-CIGS (CIGS: copper indium gallium selenide) tandems are in thin-film-form, suitable for flexible demonstrations but the bottom CIGS cell has an irregularly rough surface, posing challenges for perovskite top cell fabrication.[3] While a perovskite-perovskite tandem is also in thin-film form and can be fabricated by solution processes, the low bandgap Sn-Pb-based perovskite bottom cell is unstable due to the tendency for Sn^{2+} to oxidize into Sn^{4+}.[4] This instability has been observed in complete devices, during cell fabrication (e.g., during the crystallization of Sn-Pb perovskite film) and even during the handling of perovskite precursor pre-fabrication. This may cause a reliability issue for industrial production of perovskite-perovskite tandem.

Perovskite-OPV tandem is promising, as OPV is also a solution-processable photovoltaic technology, with a longer history of development than perovskite cell technology.[5] In the last 5 years, OPV has gained a renewed interest, as the efficiency of non-fullerene acceptor-based OPV rose from 11.2% (certified) in 2016 to 19.2% (certified) in 2023.[1] Both the energy levels and the bandgaps of OPV are tunable, rendering great flexibility for solution-processable tandem applications. In addition, low bandgap (≈1.3 eV) non-fullerene OPV cells are more stable than low bandgap (1.25 eV) Sn-Pb-based perovskites. The former has a projected lifetime of 22 years.[6] Therefore, it is advantageous to combine low-bandgap OPV with high-bandgap perovskite for high-efficiency tandems, and to date, only few demonstrations have been reported for perovskite-OPV tandems.[7–16] To realize the full potential perovskite-OPV tandems, it is imperative to further increase the efficiency of high bandgap perovskite solar cells.

In recent years, the use of self-assembled monolayer (SAM) type hole selective layers (HSLs) in perovskite solar cells for perovskite-tandems[13,17–26] have resulted in impressive power conversion efficiencies (PCEs). The benefits of SAM HSLs are wide-ranging.[17,18] They include improving morphology and crystallinity of the perovskite layer when deposited onto a SAM; changing the work function of the HSL or the perovskite layer due to insertion of dipole moment thereby improving charge selectivity or transport; improving conductivity; suppressing interface recombination, and charge accumulation thereby improving voltage output and fill factor of the cells. SAM HSLs are also ultrathin (<5 nm), compared to conventional HSLs (≈10–20 nm) requiring less material usage, and therefore are potentially more cost-effective.

Moving forward, the device performance of SAM HSL-based high bandgap perovskite cell can be further enhanced by reducing the energetic barrier and/or by introducing surface passivation at the perovskite-SAM interface. From the design principle, the additional surface passivation layer should also downshift the highest occupied molecular orbital (HOMO) level of the SAM-HSL closer to the valence band (VB) level of perovskite for carrier transport without compromising the enabling properties of the SAM interfacing with the underlying transparent conductive oxide (TCO) surface. In this regard, polycyclic aromatic hydrocarbon (PAH) passivation is very promising. As the size of the PAH is substantial enough, it can accommodate a large separation between positive and negative charges in itself resulting in a high dipole moment.[27] This causes a potential energy step or work function change ($\Delta\Phi$) of the SAM-HSL which is proportional to its dipole moment (μ) according to the Helmholtz relationship.[28] Therefore, a large positive dipole moment of a PAH compound can shift the Fermi level[17] of HSL-SAM downwards (making it more *p*-type) favoring hole extraction from the perovskite layer. In addition, PAH compounds themselves have strong self-assembling property due to the presence of π-conjugated molecules.[29,30] Their use for perovskite solar cells has been reported for bulk perovskite doping,[31,32] and as hole transport layers.[33–39]

Most recently, naphthylmethylammonium iodide (NMA-I), a PAH, has been reported for double-sided surface passivation[40] in n–i–p mid-bandgap (1.52 eV) perovskite cells producing reasonably good cell performance (23% PCE). They are yet to be utilized for p–i–n devices which are more favorable than n–i–p cells for perovskite-based tandem application, as the former typically have less optically absorptive transport layers on the sun-facing side.[41] In this work, we chose NA—Cl for their novel use in perovskite cells because it exhibits high molecular dipole moment (+8 debye) and polarizability (≈106) confirmed by density functional theory (DFT) calculations, which can induce a surface dipole[42] at the perovskite/SAM-HSL interface while retaining its self-organizing surface property on an indium tin oxide (ITO)/glass substrate. NA—Cl-induced surface modification reduces the energetic barrier for hole extraction by 210 meV compared to pristine SAM-based cells by downshifting the HOMO level of HSL closer to the perovskite VBM for cascaded charge transfer. The perovskite bandgap is also slightly blue-shifted due to the partial diffusion of Cl from NA—Cl layer into the perovskite film for bulk and interface passivation, as confirmed by time-of-flight secondary ion mass spectrometry (ToF-SIMS), thermal admittance spectroscopy (TAS), light-intensity, and temperature-dependent V_{OC} characterizations, transient absorption, and electrochemical impedance spectroscopy. As a result, NA—Cl/SAM-HSL based single-junction high bandgap inverted devices produced significant V_{OC} (≈80 mV absolute) and FF (≈4.5% absolute) improvement compared to control cells. The champion cell produces a PCE of 19.7% and a FF of 85.4%. The FF achieved in our work is the highest for a 1.78 eV single-junction perovskite cell[43] and for high bandgap cells used for

Z. Li, H. T. Nguyen
School of Engineering
The Australian National University
ACT 2601, Australia

L. Yang, J. Cairney
Australian Centre for Microscopy and Microanalysis (ACMM)
The University of Sydney
Sydney, NSW 2006, Australia

L. Yang
School of Civil and Environmental Engineering
University of Technology Sydney
81 Broadway Ultimo, NSW 2007, Australia

N. Novikova, T. Smith
School of Chemistry
The University of Melbourne
Victoria 3010, Australia

M. Jankovec
Faculty of Electrical Engineering
University of Ljubljana
Trzaska 25, Ljubljana 1000, Slovenia

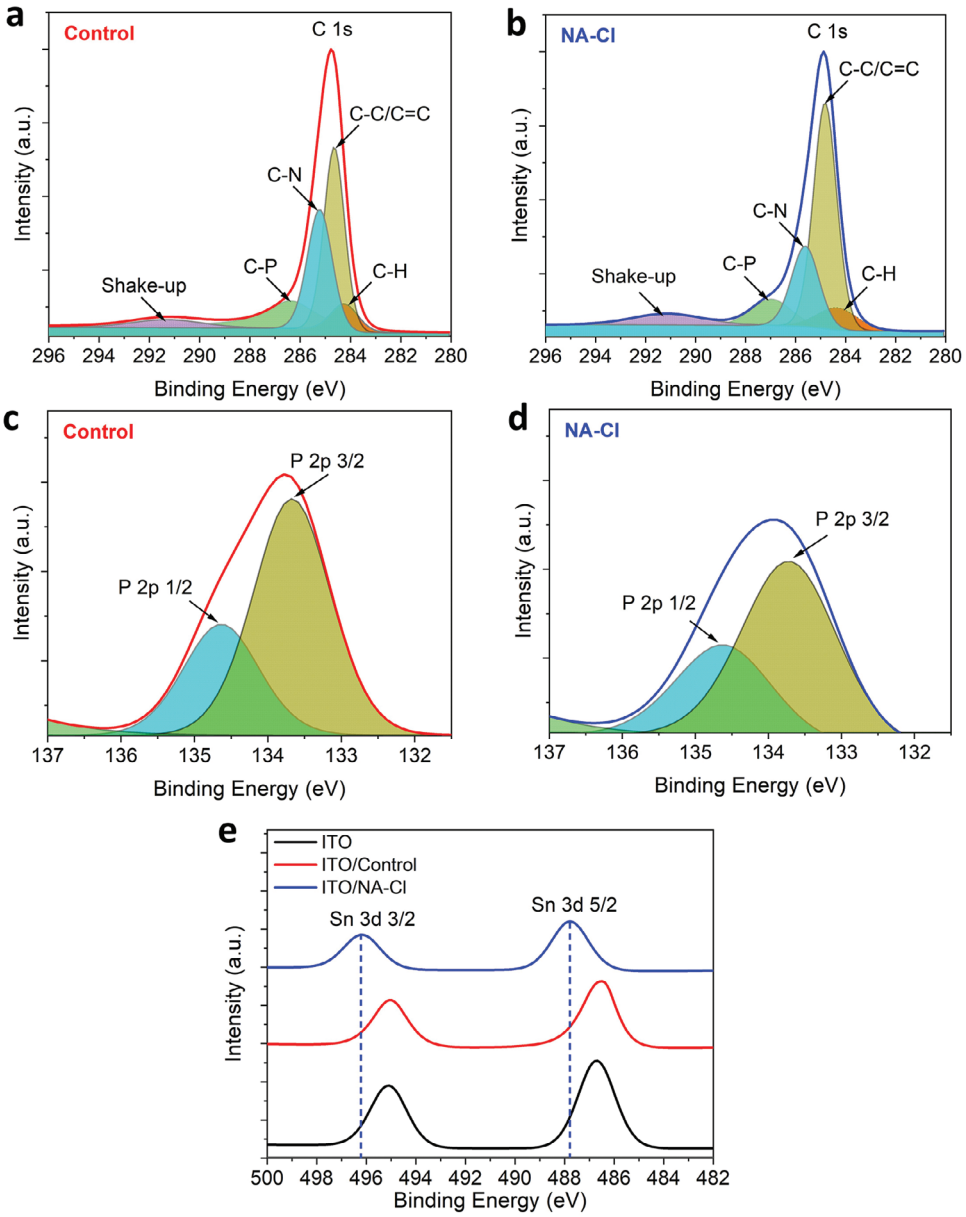

Figure 1. High-resolution X-ray photoelectron spectroscopy (XPS) spectra of a,b). C 1s, c,d). P 2p, and e. Sn 3d for untreated (Control) and NA—Cl-treated MeO-2PACz films.

perovskite-OPV tandem cells (Figure S1a,b and Table S1, Supporting Information). This is due to the very low band-offset between perovskite VBM and HSL HOMO (Figure S1f, Supporting Information).

When incorporated in a perovskite-OPV tandem cell structure, the NA—Cl treatment of HSL renders a champion power conversion efficiency (PCE) of 23% and an outstanding FF of 84%, the highest amongst those of perovskite-OPV tandem solar cells reported (Table S1, Supporting Information). This work will encourage future developments of functionalized PAH compounds for efficient high-bandgap perovskite and perovskite-based tandem solar cells.

2. Results and Discussion

To compare the surface properties of untreated (termed as "Control") and NA—Cl-treated (termed as "NA—Cl") SAM which is MeO-2PACz ([2-(3,6-Dimethoxy-9H-carbazol-9-yl)ethyl]phosphonic Acid), we compared X-ray photoelectron spectroscopy (XPS) spectra of both films. The atomic percentages of C—C/C=C, C—N, C—P, and C—H bonds[17] can be deduced from the de-convoluted peaks of high-resolution C 1s XPS (**Figure** 1a,b)) and are listed in Table S2 (Supporting Information). The atomic percentages of P 2p 1/2 and P 2p 3/2 can be deduced from the de-convolution of high-resolution P 2p

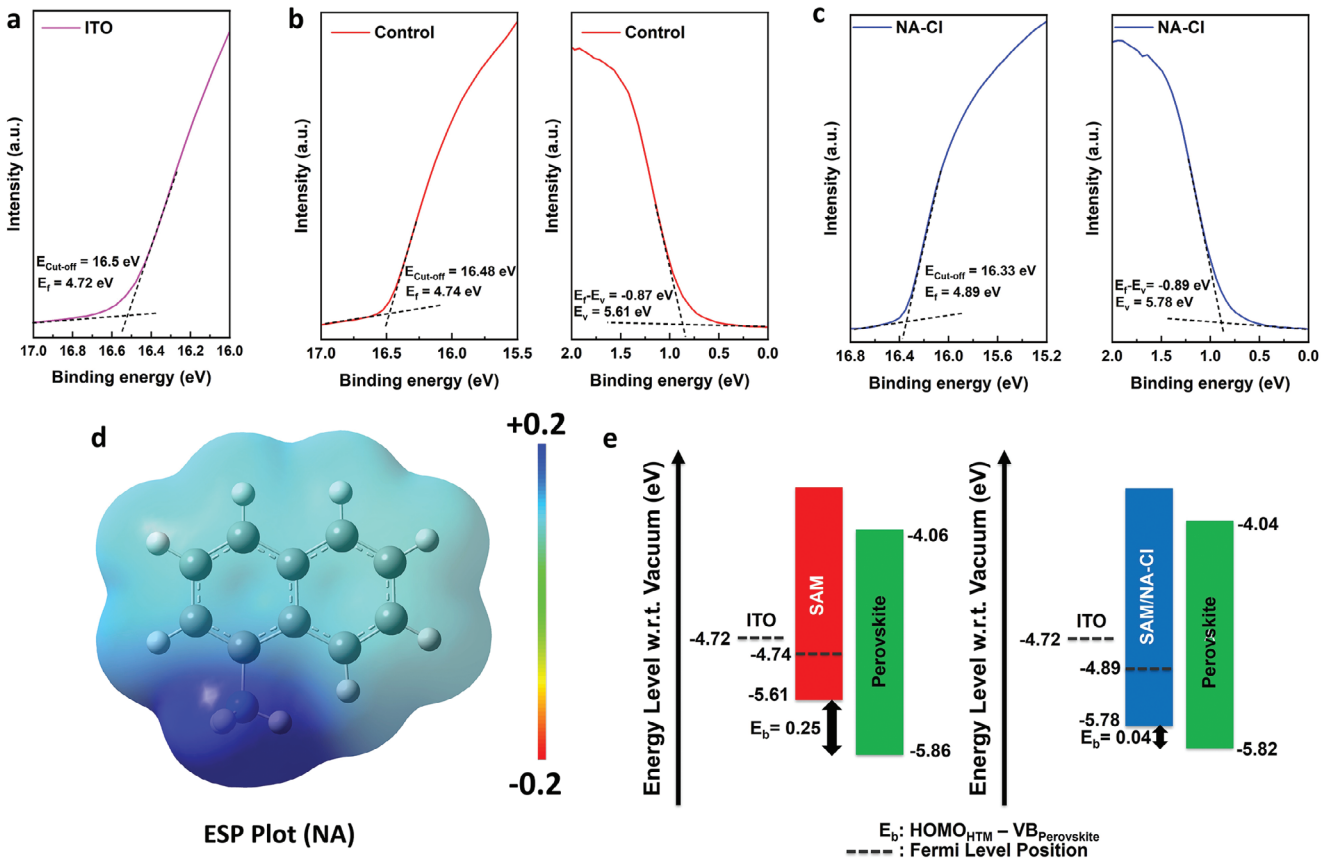

Figure 2. Ultraviolet photoelectron spectroscopies (UPS) of a) ITO, b) the untreated SAM (Control), and c) NA—Cl treated SAM. d) Electrostatic surface potential (ESP) plot of NA—Cl. e) Energetic diagrams ITO/SAM/perovskite and ITO/SAM/NA—Cl/perovskite stacks. HOMO levels with respect to E_{vac}, are 5.61, 5.78 eV, and 5.82 to 5.86 for the untreated SAM (Control), NA—Cl treated SAM, and the perovskite absorber, respectively.

XPS spectra (Figure 1c,d) and are listed in Table S2 (Supporting Information) as well. As expected, there is evidence for the presence of Cl on the NA—Cl treated SAM (Table S2, Supporting Information) even after a post-deposition-anneal (details in Supporting Information), the presence of C—C/C=C, C—N, C—P, and C—H bonds[17] (deduced from the de-convoluted peaks of high-resolution C 1s XPS (Figure 1a,b)) in NA—Cl treated SAM is encouraging suggesting that NA—Cl treated SAM did not lose its self-assembly property. Other evidence of surface modification by NA—Cl is the observed changes of atomic percentages, notably for C—C/C=C, C—P, C—N, P 2p 1/2, and P 2p 3/2 (Table S2, Supporting Information). The higher atomic percentage of C—C/C=C in NA—Cl treated SAM compared to the control is due to the additional carbon introduced. On the other hand, the atomic percentages of C—P, C—N, and P 2p are lower on the NA—Cl treated SAM, as the addition of NA—Cl reduces the proportion of P atom in the final layer and the NA—Cl treated SAM has fewer proportion of C—N bonds compared to the SAM layer. We also observed a peak shift in the Sn 3d spectra to higher binding energy (Figure 1e) for NA—Cl indicating higher oxidation states of relevant species in NA—Cl compared to the Control. The presence of higher oxidation-state species in the NA—Cl film suggests a possible work-function increase[28,44] with respect to the Control. To confirm this, we conducted ultra-violet photoelectron spectroscopy (UPS) characterization of an ITO, the Control, and NA—Cl films (**Figure 2**a,c). The work-function for SAM was −4.74 eV vs −4.72 eV for the ITO (Figure 2e). The work function was further shifted to −4.89 eV after NA—Cl treatment. We also observed a downshift of the HOMO level from −5.61 for the Control to −5.78 for the NA—Cl film (see Supporting Information for details on calculation).

A reason for the work-function change after NA—Cl treatment is its increased dipole strength increasing the minimum thermodynamic energy required to remove an electron from its surface. This is also consistent with the previous report of work-function change associated with the treatment of SAM with a PAH compound.[27] To illustrate this, we conducted a DFT simulation for illustrating (Figure 2d) the electrostatic surface potential (ESP)[45] of NA (electronegative inorganic Cl^- not shown) for showing the charge density distribution in its molecular structure. We observed a higher density of localized positive charges near the NH_3^+ group, while the charge density somewhat reduces near the polycyclic aromatic hydrocarbon ring due to their larger interatomic spatial separation in the molecular structure of NMA. From the DFT simulation, we calculated a high polarizability for NA—Cl (≈106). This suggests that an external electric field can easily distort the negative cloud of electrons in NA—Cl around its positive atomic nuclei in a direction opposite to the external field. This charge separation makes one side of the NA—Cl molecular structure positive and the opposite side negative,

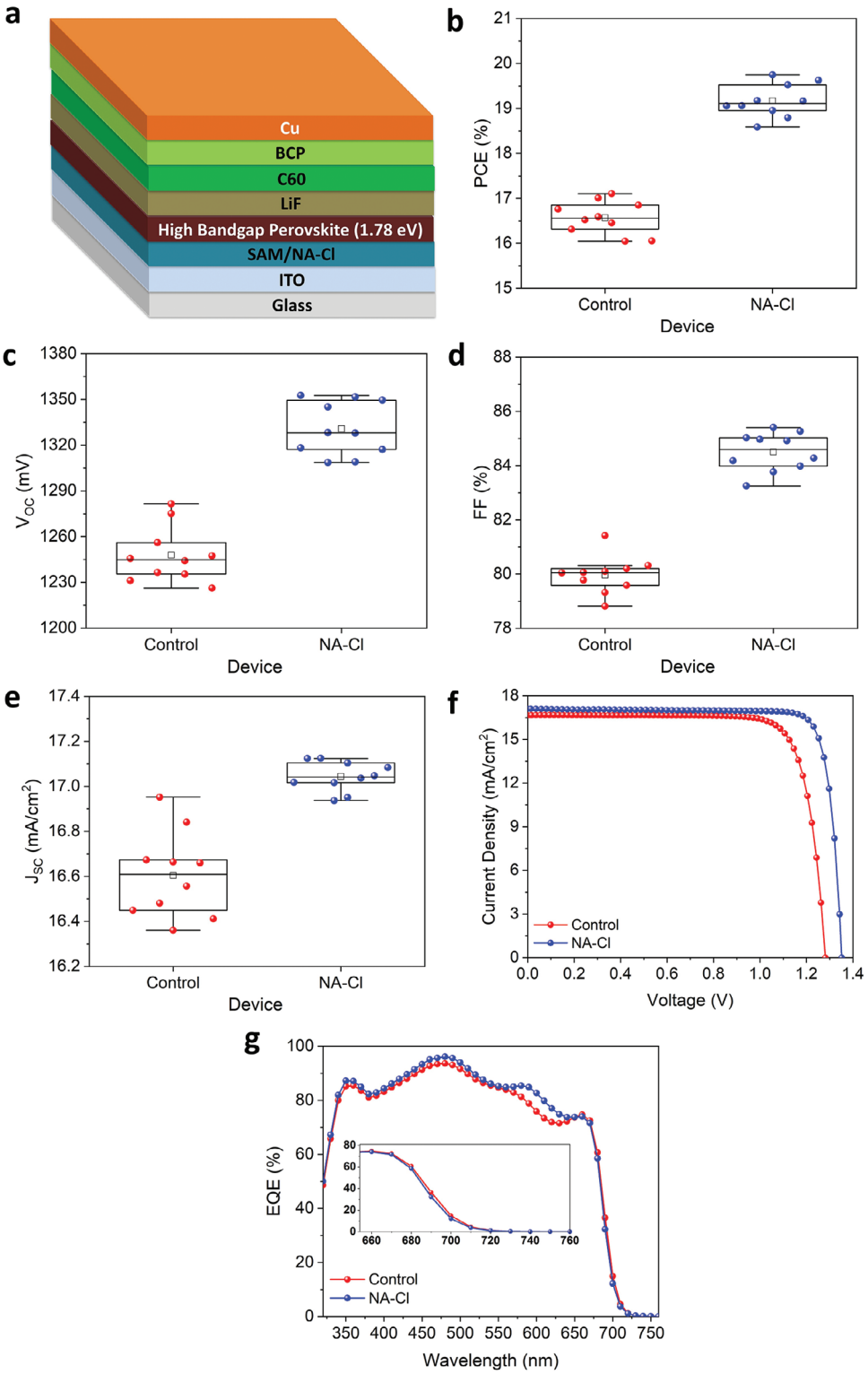

Figure 3. a) Schematic diagram of the high bandgap (1.78) single-junction perovskite p–i–n cell structure using NA—Cl-treated SAM-HSL. Distributions of b) PCE, c) V_{OC}, d) FF, and e) J_{SC} of the cells (10 cells of each kind) using untreated (Control) or NA—Cl treated SAM-HSL, f) reverse scan *J–V* curves, and g) external quantum efficiencies (EQE) curves of the respective champion cells.

Table 1. Photovoltaic parameters of single-junction high bandgap (1.78 eV) perovskite solar cells – averaged (from 10 cells) and measured for the champion device in each category: "Control" (un-treated SAM (MeO-2PACz)), and "NA—Cl" (using NA—Cl treated SAM).

Device	Average/Champion		V_{OC} [mV]	J_{SC} [mA cm^{-2}]	FF [%]	PCE [%]
Control	Average		1248 ± 18	16.6 ± 0.2	80.0 ± 0.7	16.6 ± 0.4
	Champion	Reverse	1282	16.7	79.3	17.1
		Forward	1244	16.7	79.3	16.5
NA—Cl	Average		1331 ± 17	17.0 ± 0.1	84.5 ± 0.7	19.2 ± 0.4
	Champion	Reverse	1352	17.1	85.4	19.7
		Forward	1345	17.0	83.8	19.2

creating a surface dipole[42] at the interface between perovskite and SAM. This is also consistent with a strong dipole moment calculated for NA from the DFT simulation (+8 debye), as the dipole moment quantifies the separation between positive and negative charges within a molecular system. The calculated dipole moment of NA—Cl is significantly higher than that of MeO-2PACz (+0.2 debye) reported in previous literature.[17]

The NA-Cl-induced surface dipole formation at the interface between perovskite and SAM corroborates to the downshift in HOMO[42] of NA—Cl film compared to Control. The presence of an electronegative halogen component (Cl) in NA—Cl also contributes to the deepening of HOMO.[27,46] The downshifted HOMO in NA—Cl will provide better band-offset with the valence band of a 1.78 eV perovskite (Figure S2, Supporting Information), for hole extraction by reducing the energetic barrier by 0.21 eV with respect to Control (Figure 2e).

We therefore fabricated single-junction p–i–n structure high bandgap (1.78 eV) perovskite solar cells (**Figure 3a**; Figure S3, Supporting Information) using NA—Cl treated MeO-2PACz and compared their device performance without the treatment (Control). Details of device fabrication can be found in the Supporting Information. The distributions of photovoltaic parameters are presented in Figure 3b,e while reverse and forward-scanned *J*–*V* curves and their parameters can be found in Figure S4 (Supporting Information) and **Table 1**, respectively. The best-performing cell using NA—Cl treated SAM-HSL produced a reverse scan power conversion efficiency (PCE) of 19.7% (Table 1) representing 2.6% absolute efficiency enhancement compared to the Control due to enhancement in all parameters: V_{OC} (by 70 mV), FF (by 6.1% absolute), and J_{SC} (by 0.4 mA cm^{-2}).

V_{OC} enhancement is consistent with the enhanced PL intensity observed in the steady-state photoluminescence (PL) and PL image of the perovskite film on NA—Cl-treated-SAM-HSL compared to the Control (Figure S5, Supporting Information). This is expected as PL intensity is related to the quasi-Fermi level splitting through the known Planck's generalized emission law.[47]

We also observed a very small blue-shift in the steady-state PL peak of the perovskite film on NA—Cl-treated-SAM-HSL (Figure 3g inset; Figure S5a, Supporting Information). The small increase in the perovskite bandgap (by 0.05 eV) on NA—Cl treated HSL was due to the diffusion of Cl into the perovskite evident by its high-resolution Pb 4f XPS spectra showing peaks shift to higher binding energies due to stronger electronegativity of Cl (than I)[48] (cf. Figure S6a,b, Supporting Information), indicating the presence of Cl in perovskite. This is further confirmed by results of time-of-flight secondary ion mass spectrometry (ToF-SIMS) showing the presence of Cl^- in the perovskite in NA—Cl treated devices (Figure S6d, Supporting Information). However, Cl^- was not found in the Control devices (Figure S6c, Supporting Information). Cl^- anion diffusion into the perovskite film from NA—Cl is possible due to its small ionic radii[49–51] although its effect on its XRD is almost negligible (Figure S7, Supporting Information).

Regarding J_{SC} enhancement, it is also shown in the external quantum efficiency (EQE) curve of the NA—Cl cell (Figure 3g). This is due to the reduced reflectance (Figure S8a, Supporting Information) of the cell across a relatively broad wavelength range with the presence of the NA—Cl in the hole transport layer stack possibly modifying its refractive index that better matches that of the perovskite layer thereby reducing Fresnel reflection. The improved IQE (Figure S8b, Supporting Information) across a relatively broad wavelength range also contributes to higher J_{SC}. This is due to better bulk film quality from increased grain size (Figure S9c,d, Supporting Information) and smoother surface (Figure S9e,f, Supporting Information).

FF improvement in NA–Cl treated cells came from higher R_{SH} (Figure S10b, Supporting Information) and reduced R_S (Figure S10a, Supporting Information) due to faster extraction times (Figure S10c, Supporting Information) resulting in lower transport losses (1% in a NA—Cl treated cell as opposed to 4% in the Control) (Figure S11b, Supporting Information). This is due to the more favorable band alignment[18] in the perovskite/NA—Cl/SAM stack compared to the Control. Therefore, the NA—Cl treatment reported here or its variant can be used for future demonstrations of high bandgap (1.74–1.85 eV) perovskite solar cells[52–63] to achieve higher fill factors than present values (Figure S12, Supporting Information), crucial for obtaining high efficiencies.

FF and V_{OC} enhancement are also results of better carrier lifetime observed in the perovskite film after HSL-NA—Cl treatment compared to the Control (**Figure 4a**; Table S3, Supporting Information). This is due to the suppression of trap-assisted Shockley–Read–Hall recombination[64–66] in the NA—Cl device as shown by the reduction in its ideality factor (n), to 1.2 from 1.8, as shown in the light intensity-dependent V_{OC} plot in Figure 4b. While suppressed recombination is evident in results from electrochemical impedance analyses (Figure S13 and Table S4, Supporting Information) of the solar cells, the reduction of traps is evident from results of thermal admittance spectroscopy (TAS)[67,68] (Figure 4c) of the cells showing larger reduction in trap state densities at Et_1 (0.349 eV) and Et_2 (0.355 eV) and to smaller extent, a reduction of trap state density at Et_3 (0.369 eV) in the "NA—Cl" device

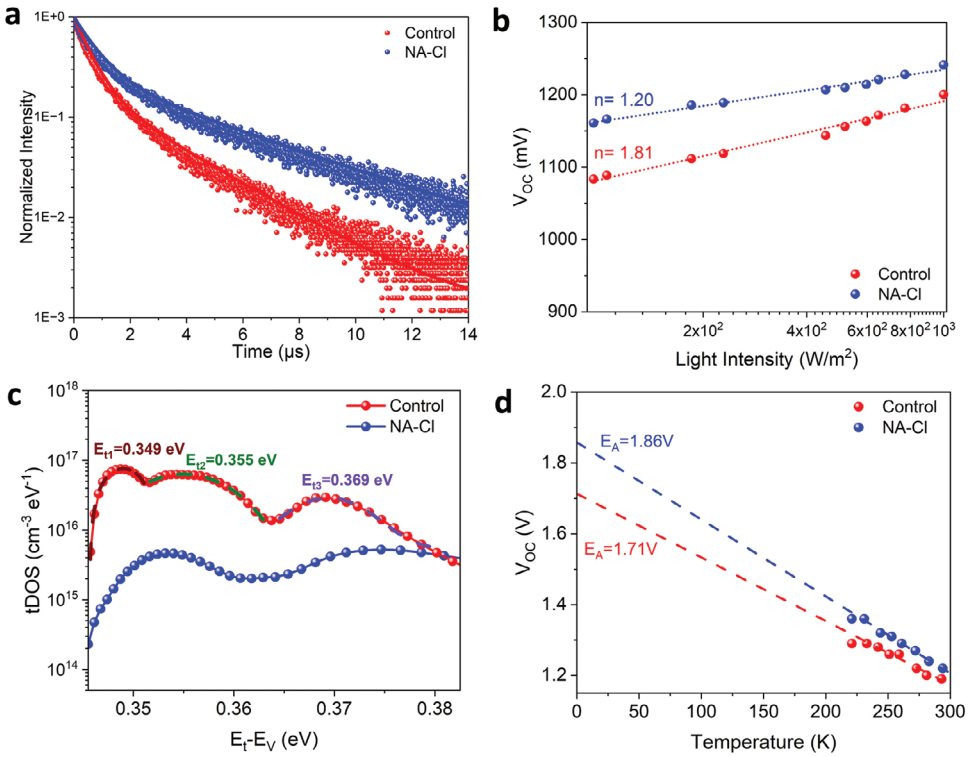

Figure 4. a) Time-resolved photoluminescence (TRPL) experimental and fitted curves of the same perovskite films, b) Light intensity-dependent V_{OC} plot for determining the ideality factors (n) (slopes of the fitted lines), c) Thermal admittance spectroscopy (TAS) of Control and NA—Cl based cells showing their densities of defect states at energy levels with respect to their valence bands, and d) Temperature-dependent V_{OC} plot for determining the activation-energies (E_a) of recombination currents (*y*-axis intercept at 0 K).

compared to the Control. The Mott–Schottky plot for determining the built-in potentials is shown in Figure S14 (Supporting Information). The energy level of the trap states is relative to the valance band.[68]

From the temperature-dependent V_{OC} measurements (Figure 4d), the recombination current activation-energy (E_a) of recombination current increased from 1.71 eV for the Control cell to 1.86 eV for the "NA—Cl" device indicating that the recombination mechanism shifted from surface-dominated in the Control to bulk-dominated[61,65,67,69,70] in the cell with HSL-NA—Cl treatment. This suggests that NA–Cl treatment improved the SAM/perovskite interface.

Therefore, HSL-NA—Cl treatment contributed to cell performance improvement mainly by improving the SAM/perovskite interface (that led to the reduction of Et_1 and Et_2 trap states) and to a smaller extent by Cl^- diffusion into the bulk,[71,72] evident by the small in blue-shift in the bandgap.[50,73,74] The diffused Cl^- could possibly passivate defects in the perovskite film,[73,75] that that led to the reduction of Et_3 trap states.

Transient absorption (TA) spectroscopy was also performed. Results are shown in Figure S15 (Supporting Information) (for excitation from the perovskite side), Figure S16 (Supporting Information) (for excitation from the glass side), and Figure S17 (Supporting Information) (global analysis) for determining corresponding decay times as listed in Table S5 (Supporting Information). Results can be interpreted by tentatively assigning 3 components (τ_2, τ_3, and τ_4 in Table S5, Supporting Information) related to various carrier decay pathways (e.g. electron, hole, and bulk recombinations). Long decay lifetimes (for both τ_2 and τ_3) can be observed in the presence of NA—Cl and especially when the sample was illuminated from the glass side, the side that is closest to the SAM. τ_2 increased from 22 to 130 ps while τ_3 increased from 103 to 622 ps. This is an indicator of a better SAM/perovskite interface. Even when the sample was illuminated from the perovskite side, far from the SAM side, τ_2 and τ_3 also increased although by a smaller extent, from 38 to 50 ps and from 349 to 376 ps, respectively suggesting improvement in the bulk.

Inspired by the improved performance of the single-junction high bandgap (1.78 V) p–i–n perovskite solar cells using HSL-NA—Cl treatment, we employed these cells for the demonstration of perovskite-OPV tandems (**Figure 5a**; Figure S18, Supporting Information).

For the OPV cell (Figure S19a, Supporting Information), $(C_{68}H_{76}F_2O_2S_8)_n$: $C_{82}H_{86}F_4N_8O_2S_5$ (PM6:Y6) donor–acceptor based binary[7] was used due to excellent absorption of near-IR (infra-red) wavelengths. Details of OPV device fabrication can be found in the Supporting Information. The distribution of photovoltaic parameters of single-junction OPV cells are presented in Figure S19b,h and in Table S6 (Supporting Information). The champion OPV cell demonstrated a PCE of 16.8% under reverse scan (Figure S19b and Table S6, Supporting Information).

For interfacing between the perovskite and OPV sub-cells in tandem, a LiF/C_{60}/ALD SnO_2/thin Au stack was used. The distribution of photovoltaic parameters for the tandem cells can be

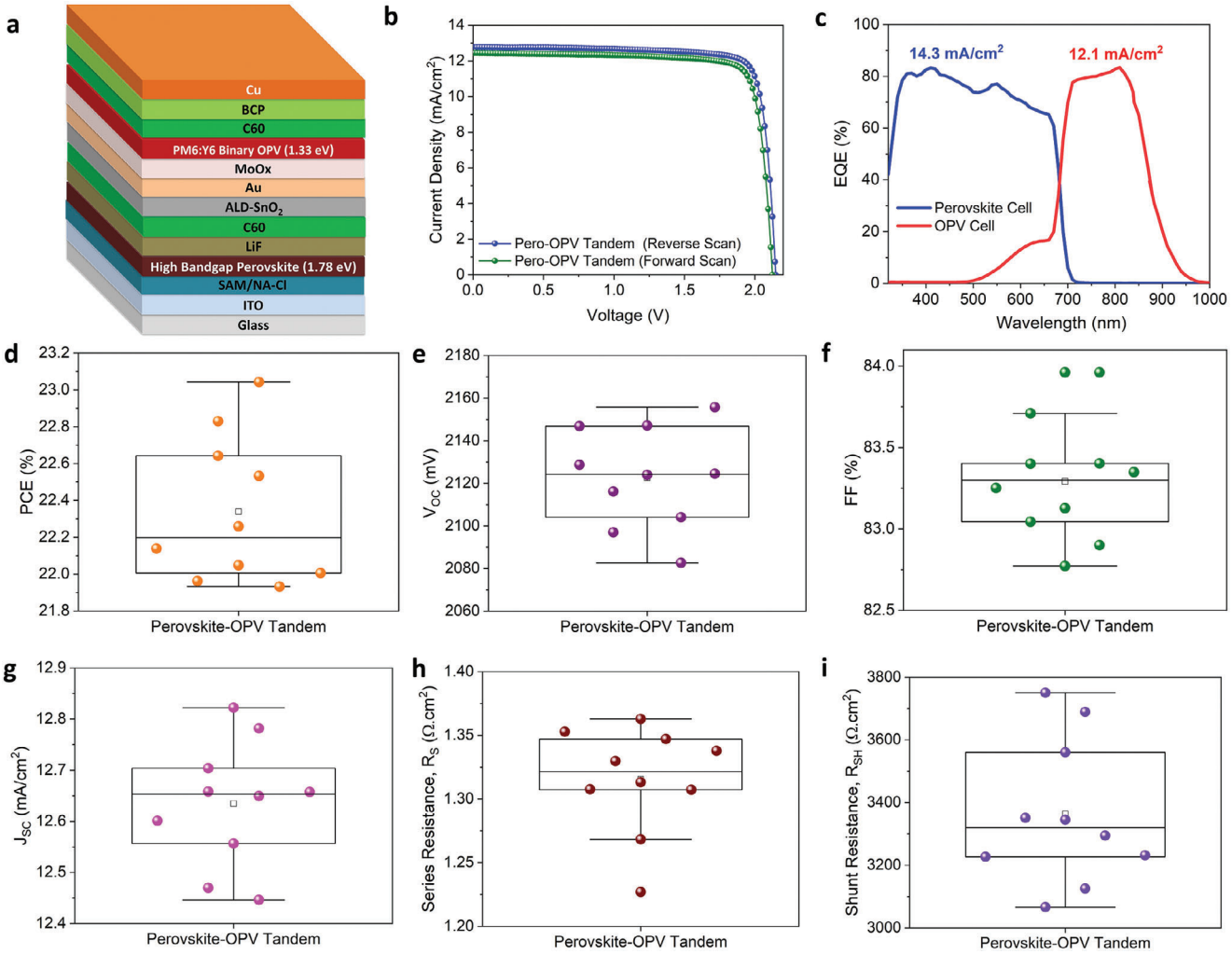

Figure 5. a) Schematic diagram of the p–i–n perovskite-OPV tandem solar cell structure consisting of low bandgap (1.33 eV) OPV and high bandgap (1.78 eV) Pb-based perovskite using NA–Cl treated SAM. b) *J–V* curves of the champion tandem cell under reverse and forward scans. c) EQE curves of OPV and perovskite subcells in a representative tandem. Distributions of d) PCE, e) V_{OC}, f) FF, g) J_{SC}, h) R_S, and i) R_{SH} of tandem solar cells (10 cells).

found in Figure 5d-i. The champion tandem cell produced a reverse scan efficiency of 23% with V_{OC} comparable to those of the state-of-the-arts (Table S1, Supporting Information) and a record FF of 84% (**Table 2**). We also fabricated larger area (1 cm^2) tandem solar cells achieving 20.2% efficiency with V_{OC}, J_{SC}, and FF values of 2.02 V, 79.3%, and 12.7 mA cm^{-2}, respectively (Figure S20, Supporting Information).

While the lower current flow inherent in tandem cells due to the "sectioning" of the solar spectrum helps to reduce R_S, the lower R_S demonstrated also shows the effectiveness of the ALD-SnO_2/Au as an interlayer stack integrating the perovskite and OPV cells for tandems. Another contributor to high FF is the current mismatch between perovskite and OPV subcells. Preliminary work was then subsequently conducted attempting to over the current mismatch by increasing the OPV blend concentration from 15 to 17 mg mL^{-1} while keeping the donor and acceptor ratio the same as before (1:1.5). 24.2% efficiency was achieved for a perovskite-OPV tandem (Figure S21, Supporting Information). In the future, current mismatch between subcells can be further overcome for even higher efficiency by widening the bandgap of the perovskite top cell[21,23,24,76,77] or lowering the bandgap of OPV subcell bandgap (to ≈1.2 eV) although not-trivial and also by replacing the highly absorptive metal (Au) interconnection layer with a more transparent ultra-thin (1 to 4 nm) indium tin or indium zinc oxide layer[13,15] to reduce optical loss thereby increasing $J_{SC\ tandem}$. It is anticipated FF_{tandem} can further be improved if R_S from the OPV cell can be further reduced (c.f. Figure S19g with Figure S10a, Supporting Information).

Table 2. Photovoltaic parameters of perovskite-OPV tandem solar cells – averaged (from 15 cells) and measured for the champion device.

Average/Champion		V_{OC} [mV]	J_{SC}[mA cm^{-2}]	FF [%]	PCE [%]
Average		2122 ± 23	12.6 ± 0.1	83.3 ± 0.4	22.3 ± 0.4
Champion	Reverse	2147	12.8	84.0	23.0
	Forward	2123	12.4	83.4	22.1

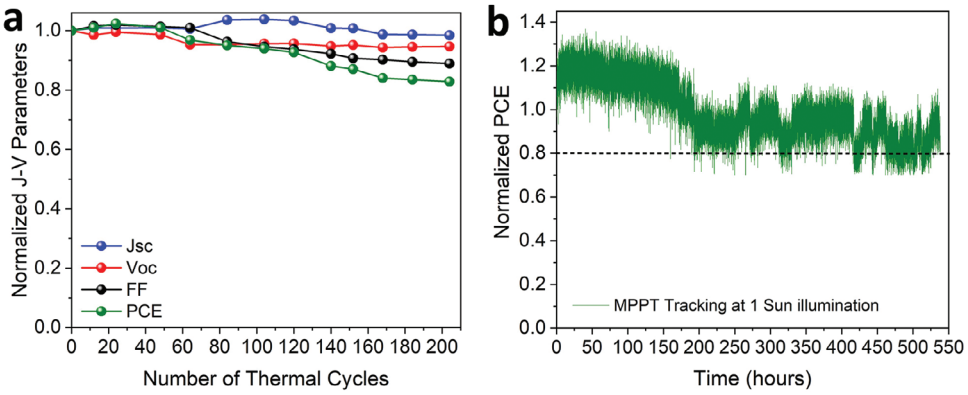

Figure 6. a) Thermal cycling (between −40 and 85°C), and b) maximum power point tracking under 1 sun illumination of an encapsulated perovskite-OPV tandem solar cell.

Unencapsulated tandems (Figure S22, Supporting Information) of both types suffer from poor durability even under ambient (20–25 °C, dark, 20–30% relative humidity) storage due to more rapid degradation in the OPV cell (cf. Figures S23 and S22, Supporting Information). However, an encapsulated tandem cell retained 83% of initial efficiency after 200 thermal cycles (**Figure 6a**). This is the first time a perovskite-OPV tandem is assessed by the International Electrotechnical Commission (IEC) thermal cycling test. A tandem cell also demonstrated >80% of initial efficiency after 540 h of maximum power point tracking under continuous 1 sun illumination (Figure 6b). Clearly, there is room for improvement in terms of durability. One approach may involve replacing MoO_X hole transport layer in the OPV cell with an alternative that does not degrade under thermal stress at ≈60 °C as seen in MoO_X.[78]

3. Conclusion

In summary, we reported the use of a novel polycyclic aromatic hydrocarbon-based surface modifier and passivation layer (NA—Cl) for SAM-based HSL for the demonstration of high bandgap (1.78 eV) inverted perovskite and perovskite-OPV tandem solar cells. While NA—Cl retained the self-organization property of SAM, it exhibited high polarizability and dipole moment forming a surface dipole at the perovskite/HSL interface. This downshifted the HOMO level thereby reducing the energetic barrier for hole extraction by 210 meV relative to the perovskite valence band. While solar device performance improvement was mainly due to the improvement of the perovskite/HSL interface, Cl^- diffusion from the NA—Cl to the bulk in the vicinity of the surface also contributed to bulk passivation. This HSL-NA—Cl treatment is therefore highly effective and is compatible for p–i–n and high bandgap solar cell resulting in V_{OC}, FF, and J_{SC} enhancements. When implemented in a perovskite-OPV tandem, the champion NA—Cl-based tandem cell demonstrated a PCE of 23% with an outstanding FF of 84%, which was the highest for perovskite-OPV tandem cells at the time of reporting. These results are highly relevant to future developments of high-efficiency single-junction high bandgap perovskite and perovskite-based tandem solar cells by the functionalization of polycyclic aromatic hydrocarbon-based compound for interface engineering.

Supporting Information

Supporting Information is available from the Wiley Online Library or from the author.

Acknowledgements

This work was supported by the Australian Government through the Australian Renewable Energy Agency (ARENA) via projects 2020 RND001, 2020 RND003, and Australian Centre for Advanced Photovoltaics; and through the Australian Research Council (ARC) via Future Fellowships FT210100210 for A. H.-B and FT180100232 for J. C. This research was supported by an AINSE Ltd. Early Career Researcher Grant (ECRG). M. A. M. also acknowledges the support of The University of Sydney Nano Institute Early Career Research Support Fund (ESF). C. L. and S. T. acknowledge the support of the John Hooke Chair of Nanoscience Postgraduate Research Scholarships. G. W. was supported by the University of Sydney International Scholarship. T. L. L was supported by the University of Sydney Faculty of Science Postgraduate Research Excellence Award. H. T. Nguyen acknowledges the support from the Australian Centre for Advanced Photovoltaics (ACAP) Infrastructure Fund. A. H.-B., M. A. M. and J. Z. acknowledge the support of the University of Sydney – University College London Partnership Collaboration Awards for this work. The authors acknowledge the facilities and the scientific and technical assistance of Sydney Analytical, a core research facility at The University of Sydney. The authors also acknowledge the technical and scientific assistance provided by i) Research & Prototype Foundry Core Research Facility at the University of Sydney, part of the Australian National Fabrication Facility, ii) Sydney Microscopy & Microanalysis, the University of Sydney node of Microscopy Australia, iii) Electron Microscopy Unit at University of New South Wales (UNSW), and iv) Surface Analysis Laboratory, Solid State & Elemental Analysis Unit at Mark Wainwright Analytical Centre at UNSW.

Conflict of Interest

The authors declare no conflict of interest.

Author Contributions

A.M. and J.Z. contributed equally to this work. A.H.-B. and M.A.M. conceived and designed all the experimental work. M.A.M. conducted device

fabrications. M.A.M., J.Z., C.L., G.W., S.T., J.B., Z.L., L.Y., T.L.L., J.Y., N.N., and H.T.N. performed device and film characterizations. H.C. contributed to device encapsulation. M.H.R. and A.U. contributed to OPV cell development. The manuscript was written by M.A.M. and A.H.-B. All authors contributed to the discussion of the data, writing of the sections of the manuscript and revision of the manuscript. The overall project was supervised by A.H.-B.

Data Availability Statement

Research data are not shared.

Keywords

dipole moment, perovskite-OPV tandem solar cell, polycyclic aromatic hydrocarbon, passivation

Received: February 9, 2024
Revised: October 4, 2024
Published online: November 3, 2024

[1] NREL Best Research Cell Efficiency Chart, https://www.nrel.gov/pv/cell-efficiency.html (acccessed: October 2024).
[2] M. A. Green, A. Ho-Baillie, H. J. Snaith, *Nat. Photonics* **2014**, *8*, 506.
[3] A. W. Y. Ho-Baillie, J. Zheng, M. A. Mahmud, FJ Ma, D. R. McKenzie, M. A. Green, *Appl. Phys. Rev. 8*, 041307, **2021**.
[4] R. Lin, K. e Xiao, Z. Qin, Q. Han, C. Zhang, M. Wei, M. I. Saidaminov, Y. Gao, J. Xu, M. Xiao, A. Li, J. Zhu, E. H. Sargent, H. Tan, *Nat. Energy* **2019**, *4*, 864.
[5] M. B. Upama, M. A. Mahmud, G. Conibeer, A. Uddin, *Sol. RRL* **2020**, *4*, 1900342.
[6] X. Xu, J. Xiao, G. Zhang, L. Wei, X. Jiao, H.-L. Yip, Y. Cao, *Sci. Bull.* **2020**, *65*, 208.
[7] X. u Chen, Z. Jia, Z. Chen, T. Jiang, L. Bai, F. Tao, J. Chen, X. Chen, T. Liu, X. Xu, C. Yang, W. Shen, W. E. I. Sha, H. Zhu, Y. (.M.). Yang, *Joule* **2020**, *4*, 1594.
[8] S. Xie, R. Xia, Z. Chen, J. Tian, L. Yan, M. Ren, Z. Li, G. Zhang, Q. Xue, H.-L. Yip, Y. Cao, *Nano Energy* **2020**, *78*, 105238.
[9] C.-C. Chen, S. H. Bae, W. H. Chang, Z. Hong, G. Li, Q. Chen, H. Zhou, Y. Yang, *Mater. Horiz.* **2015**, *2*, 203.
[10] Y. Liu, L. A. Renna, M. Bag, Z. A. Page, P. Kim, J. Choi, T. Emrick, D. Venkataraman, T. P. Russell, *ACS Appl. Mater. Interfaces* **2016**, *8*, 7070.
[11] Z. Li, S. Wu, J. Zhang, K. C. Lee, H. Lei, F. Lin, Z. Wang, Z. Zhu, A. K. Jen, *Adv. Energy Mater. 10*, 2000361, **2020**.
[12] P. Wang, W. Li, O. J. Sandberg, C. Guo, R. Sun, H. Wang, D. Li, H. Zhang, S. Cheng, D. Liu, J. Min, A. Armin, T. Wang, *Nano Lett.* **2021**, *21*, 7845.
[13] K. O. Brinkmann, T. Becker, F. Zimmermann, C. Kreusel, T. Gahlmann, M. Theisen, T. Haeger, S. Olthof, C. Tückmantel, M. Günster, T. Maschwitz, F. Göbelsmann, C. Koch, D. Hertel, P. Caprioglio, F. Peña-Camargo, L. Perdigón-Toro, A. Al-Ashouri, L. Merten, A. Hinderhofer, L. Gomell, S. Zhang, F. Schreiber, S. Albrecht, K. Meerholz, D. Neher, M. Stolterfoht, T. Riedl, *Nature* **2022**, *604*, 280.
[14] H. Xu, L. Torres Merino, M. Koc, E. Aydin, S. Zhumagali, M. d. A. Haque, A. Yazmaciyan, A. Sharma, D. Rosas Villalva, L. Huerta Hernandez, M. De Bastiani, M. Babics, F. H. Isikgor, J. Troughton, S. De Wolf, S. Yerci, D. Baran, *ACS Appl. Energy Mater.* **2022**, *5*, 14035.
[15] W. Chen, Y. Zhu, J. Xiu, G. Chen, H. Liang, S. Liu, H. Xue, E. Birgersson, J. W. Ho, X. Qin, J. Lin, R. Ma, T. Liu, Y. He, A. M.-C. Ng, X. Guo, Z. He, H. e Yan, A. B. Djurisic, Y. i Hou, *Nat. Energy* **2022**, *7*, 229.
[16] Z. Zhang, C. Cueto, Y. Ding, L. Yu, T. P. Russell, T. Emrick, Y. Liu, *ACS Appl. Mater. Interfaces* **2022**, *14*, 29896.
[17] A. Al-Ashouri, A. Magomedov, M. Roß, M. Jošt, M. Talaikis, G. Chistiakova, T. Bertram, J. A. Márquez, E. Köhnen, E. Kasparavičius, S. Levcenco, L. Gil-Escrig, C. J. Hages, R. Schlatmann, B. Rech, T. Malinauskas, T. Unold, C. A. Kaufmann, L. Korte, G. Niaura, V. Getautis, S. Albrecht, *Energy Environ. Sci.* **2019**, *12*, 3356.
[18] A. Al-Ashouri, E. Köhnen, B. Li, A. Magomedov, H. Hempel, P. Caprioglio, J. A. Márquez, A. B. M. Vilches, E. Kasparavicius, J. A. Smith, *Science* **2020**, *370*, 1300.
[19] H. Xu, L. Torres Merino, M. Koc, E. Aydin, S. Zhumagali, M. d. A. Haque, A. Yazmaciyan, A. Sharma, D. Rosas Villalva, L. Huerta Hernandez, M. De Bastiani, M. Babics, F. H. Isikgor, J. Troughton, S. De Wolf, S. Yerci, D. Baran, *ACS Appl. Energy Mater.* **2022**, *5*, 14035.
[20] J. Liu, M. D. Bastiani, E. Aydin, G. T. Harrison, Y. Gao, R. R. Pradhan, M. K. Eswaran, M. Mandal, W. Yan, A. Seitkhan, M. Babics, A. S. Subbiah, E. Ugur, F. Xu, L. Xu, M. Wang, A. Rehman, A. Razzaq, J. Kang, R. Azmi, A. A. Said, F. H. Isikgor, T. G. Allen, D. Andrienko, U. Schwingenschlögl, F. Laquai, S. D. Wolf, *Science.* **2022**, *377*, 302.
[21] S. Wu, Y. Yan, J. Yin, K. Jiang, F. Li, Z. Zeng, S.-W. Tsang, A. K.-Y. Jen, *Nat. Energy* **2024**, *9*, 411.
[22] Y. An, N. Zhang, Z. Zeng, Y. Cai, W. Jiang, F. Qi, L. Ke, F. R. Lin, S-W Tsang, T. Shi, A. K.-Y. Jen, H-L Yip, *Adv. Mater.* **2024**, *36*, 2306568.
[23] Z. Zhang, W. Chen, X. Jiang, J. Cao, H. Yang, H. Chen, F. u Yang, Y. Shen, H. Yang, Q. Cheng, X. Chen, X. Tang, S. Kang, X.-M. Ou, C. J. Brabec, Y. Li, Y. Li, *Nat. Energy* **2024**, *9*, 592.
[24] X. Guo, Z. Jia, S. Liu, R. Guo, F. Jiang, Y. Shi, Z. Dong, R. Luo, Y. u-D. Wang, Z. Shi, J. Li, J. Chen, L. K. Lee, P. Müller-Buschbaum, D. S. Ginger, D. J. Paterson, Y. i Hou, *Joule* **2024**, *8*, 2554.
[25] X. Wu, X. Wu, D. Zhang, B. Liu, Y. Wang, X. Wang, Q. Liu, D. Gao, N. Wang, B. Li, L. Wang, Z. Yu, X. Li, S. Xiao, N. Li, M. Stolterfoht, Y-H Lin, S. Yang, X. C. Zeng, Z. Zhu, *Adv. Mater.* **2024**, https://doi.org/10.1002/adma.202410692.
[26] X. Cui, G. Xie, Y. Liu, X. Xie, H. Zhang, H. Li, P. Cheng, G. Lu, L. Qiu, Z. Bo, *Adv. Mater.* **2024**, 2408646.
[27] Q. Tao, M. Xiao, M. Zhu, L. Shao, Z. Sui, P. u Wang, G. Huang, Y. Pei, W. Zhu, F. Huang, *Dyes Pigm.* **2017**, *144*, 142.
[28] J. B. Rivest, G. Li, I. D. Sharp, J. B. Neaton, D. J. Milliron, *J. Phys. Chem. Lett.* **2014**, *5*, 2450.
[29] G. E. Hicks, S. Li, N. K. Obhi, C. N. Jarrett-Wilkins, D. S. Seferos, *Adv. Mater.* **2021**, *33*, 2006287.
[30] H. Narita, H. Choi, M. Ito, N. Ando, S. Ogi, S. Yamaguchi, *Chem. Sci.* **2022**, *13*, 1484.
[31] J. Xue, R. Wang, X. Chen, C. Yao, X. Jin, K.-L. i Wang, W. Huang, T. Huang, Y. Zhao, Y. Zhai, D. Meng, S. Tan, R. Liu, Z.-K. Wang, C. Zhu, K. Zhu, M. C. Beard, Y. Yan, Y. Yang, *Science* **2021**, *371*, 636.
[32] C. Peng, X. Xia, X. Wang, J. Peng, Z. Fan, F. Li, *Appl. Surf. Sci.* **2022**, *585*, 152670.
[33] X. Deng, *Angew. Chemie.* **2022**, *61*, 202203088.
[34] Z. Tang, *ChemSusChem.* **2021**, *14*, 4923.
[35] X. Sun, Q. Xue, Z. Zhu, Q. i Xiao, K. Jiang, H.-L. Yip, H. e Yan, Z. '. Li, *Chem. Sci.* **2018**, *9*, 2698.
[36] Z. Wang, C. Xu, Z. Yang, Y. Zou, K. Zhang, P. Gao, W. Xu, G. Li, J. Chen, M. Liang, *Dyes Pigm.* **2023**, *211*, 111066.
[37] D. Chandrasekaran, Y.-L. Chiu, C.-K. Yu, Y.-S. Yen, Y.-J. Chang, *Chem.–An Asian J. 16*, 3719, **2021**.
[38] M. Pegu, *Emergent Materials* **2020**, *3*, 109.
[39] L. Liang, Y. Wang, Z. Zhang, J. Wang, K. Feng, S. Ma, Y. Li, X. Guo, P. Gao, *ACS Appl. Energy Mater.* **2021**, *4*, 1250.
[40] M. Hatamvand, S. Gholipour, M. Chen, Y. Zhou, T. Jiang, Z. Hu, Y. Chen, W. Huang, *Chem. Eng. J.* **2023**, *460*, 141788.
[41] A. Al-Ashouri, E. Köhnen, B. Li, A. Magomedov, H. Hempel, P. Caprioglio, J. A. Márquez, A. B. Morales Vilches, E. Kasparavicius, J. A. Smith, Nga Phung, D. Menzel, M. Grischek, L. Kegelmann, D.

Skroblin, C. Gollwitzer, T. Malinauskas, M. Jošt, G. Matič, B. Rech, R. Schlatmann, M. Topič, L. Korte, A. Abate, B. Stannowski, D. Neher, M. Stolterfoht, T. Unold, V. Getautis, S. Albrecht, **2020**, *370*, 1300.
[42] G. Wang, C. Wang, Y. Gao, S. Wen, R. C. I. MacKenzie, L. Guo, W. Dong, S. Ruan, *J. Energy Chem.* **2022**, *64*, 55.
[43] O. Almora, C. I. Cabrera, S. Erten-Ela, K. Forberich, K. Fukuda, F. Guo, J. Hauch, A. W. Y. Ho-Baillie, T. J. Jacobsson, R. A. J. Janssen, T. Kirchartz, M. A. Loi, X. Mathew, D. B. Mitzi, M. K. Nazeeruddin, U. W. Paetzold, B. P. Rand, U. Rau, T. Someya, E. Unger, L. Vaillant-Roca, C. J. Brabec, *Adv. Energy Mater.* **2024**, *14*, 2303173.
[44] N. Phung, M. Verheijen, A. Todinova, K. Datta, M. Verhage, A. Al-Ashouri, H. Köbler, X. Li, A. Abate, S. Albrecht, M. Creatore, *ACS Appl. Mater. Interfaces* **2022**, *14*, 2166.
[45] M. R. Janjua, *Chem. – A Europ. J.* **2021**, *27*, 4197.
[46] H. Yang, C. Cui, Y. Li, *Acc. Mater. Res.* **2021**, *2*, 986.
[47] Z. Hameiri, A. M. Soufiani, M. K. Juhl, L. Jiang, F. Huang, Y.-B. Cheng, H. Kampwerth, J. W. Weber, M. A. Green, T. Trupke, *Progr. Photovolt.: Res. Appl.* **2015**, *23*, 1697.
[48] J. Bing, D. S. Lee, Y. Cho, J. Zheng, Y. Li, S. Tang, M. Zhang, S. Huang, A. W. Y. Ho-Baillie, *Mater. Today Energy* **2020**, *18*, 100551.
[49] Z. Huang, A. H. Proppe, H. Tan, M. I. Saidaminov, F. Tan, A. Mei, C.-S. Tan, M. Wei, Y. i Hou, H. Han, S. O. Kelley, E. H. Sargent, *ACS Energy Lett.* **2019**, *4*, 1521.
[50] J. Xu, C. C. Boyd, Z. J. Yu, A. F. Palmstrom, D. J. Witter, B. W. Larson, R. M. France, J. Werner, S. P. Harvey, E. J. Wolf, W. Weigand, S. Manzoor, M. F. A. M. van Hest, J. J. Berry, J. M. Luther, Z. C. Holman, M. D. McGehee, *Science* **2020**, *367*, 1097.
[51] W. Chai, L. Li, W. Zhu, D. Chen, L. Zhou, H. Xi, J. Zhang, C. Zhang, Y. Hao, *Research* **2023**, *6*, 0196.
[52] Q. Ye, Y. Zhao, S. Mu, F. Ma, F. Gao, Z. Chu, Z. Yin, P. Gao, X. Zhang, J. You, *Adv. Mater.* **2019**, *31*, 1905143.
[53] Y. Lin, B. Chen, F. Zhao, X. Zheng, Y. Deng, Y. Shao, Y. Fang, Y. Bai, C. Wang, J. Huang, *Adv. Mater.* **2017**, *29*, 1700607.
[54] K. Xiao, Y. H. Lin, M. Zhang, R. D. Oliver, X. Wang, Z. Liu, X. Luo, J. Li, D. Lai, H. Luo, R. Lin, *Science* **2022**, *376*, 762.
[55] Y. Wang, R. Lin, X. Wang, C. Liu, Y. Ahmed, Z. Huang, Z. Zhang, H. Li, M. Zhang, Y. Gao, H. Luo, P. u Wu, H. Gao, X. Zheng, M. Li, Z. Liu, W. Kong, L. Li, K. Liu, M. I. Saidaminov, L. Zhang, H. Tan, *Nat. Commun.* **2023**, *14*, 1819.
[56] H. Chen, A. Maxwell, C. Li, S. Teale, B. Chen, T. Zhu, E. Ugur, G. Harrison, L. Grater, J. Wang, Z. Wang, L. Zeng, S. o. M. Park, L. Chen, P. Serles, R. A. Awni, B. Subedi, X. Zheng, C. Xiao, N. J. Podraza, T. Filleter, C. Liu, Y. i Yang, J. M. Luther, S. De Wolf, M. G. Kanatzidis, Y. Yan, E. H. Sargent, *Nature* **2023**, *613*, 676.
[57] J. Heo, S. W. Lee, J. Yong, H. Park, Y. u. K. Lee, J. Shin, D. R. Whang, D. W. Chang, H. J. Park, *Chem. Eng. J.* **2023**, *474*, 145632.
[58] S. Qin, C. Lu, Z. Jia, Y. Wang, S. Li, W. Lai, P. Shi, R. Wang, C. Zhu, J. Du, J. Zhang, *Adv. Mater.* **2022**, *34*, 2108829.
[59] Z. Yang, Z. Yu, H. Wei, X. Xiao, Z. Ni, B. o Chen, Y. Deng, S. N. Habisreutinger, X. Chen, K. Wang, J. Zhao, P. N. Rudd, J. J. Berry, M. C. Beard, J. Huang, *Nat. Commun.* **2019**, *10*, 4498.
[60] W.-Q. Wu, Z. Yang, P. N. Rudd, Y. Shao, X. Dai, H. Wei, J. Zhao, Y. Fang, Q. Wang, Y. Liu, Y. Deng, X. Xiao, Y. Feng, J. Huang, *Sci. Adv.* **2019**, *5*, eaav8925.
[61] M. A. Mahmud, J. Zheng, S. Tang, G. Wang, J. Bing, A. D. Bui, J. Qu, L. Yang, C. Liao, H. Chen, S. P. Bremner, H. T. Nguyen, J. Cairney, A. W. Y. Ho-Baillie, *Adv. Energy Mat.* **2022**, *12*, 2201672.
[62] R. Lin, Y. Wang, Q. Lu, B. Tang, J. Li, H. Gao, Y. Gao, H. Li, C. Ding, J. Wen, P. u Wu, C. Liu, S. Zhao, K. Xiao, Z. Liu, C. Ma, Y. Deng, L. Li, F. Fan, H. Tan, *Nature* **2023**, *620*, 994.
[63] H. Cui, L. Huang, S. Zhou, C. Wang, X. Hu, H. Guan, S. Wang, W. Shao, D. Pu, K. Dong, J. Zhou, P. Jia, W. Wang, C. Tao, W. Ke, G. Fang, *Energy Environ. Sci.* **2023**, *16*, 5992,.
[64] D. Glowienka, Y. Galagan, *Adv. Mat.* **2022**, *34*, 2105920.
[65] Y. Cho, H. D. o Kim, J. Zheng, J. Bing, Y. Li, M. Zhang, M. A. Green, A. Wakamiya, S. Huang, H. Ohkita, A. W. Y. Ho-Baillie, *ACS Energy Lett.* **2021**, *6*, 925.
[66] M. Degani, Q. An, M. Albaladejo-Siguan, Y. J. Hofstetter, C. Cho, F. Paulus, G. Grancini, Y. Vaynzof, *Sci Adv.* **2021**, *7*, eabj7930.
[67] S. Tang, J. Bing, J. Zheng, J. Tang, Y. Li, M. Mayyas, Y. Cho, T. W. Jones, T. C.-J. Yang, L. Yuan, M. Tebyetekerwa, H. T. Nguyen, M. P. Nielsen, N. J. Ekins-Daukes, K. Kalantar-Zadeh, G. J. Wilson, D. R. McKenzie, S. Huang, A. W. Y. Ho-Baillie, *Cell Rep. Phys. Sci.* **2021**, *2*, 100511.
[68] H.-S. Duan, H. Zhou, Q. i Chen, P. Sun, S. Luo, T.-B. Song, B. Bob, Y. Yang, *Phys. Chem. Chem. Phys.* **2015**, *17*, 112.
[69] W. Tress, M. Yavari, K. Domanski, P. Yadav, B. Niesen, J. P. Correa Baena, A. Hagfeldt, M. Graetzel, *Energy Environ. Sci.* **2018**, *11*, 151.
[70] M. A. Mahmud, *ACS Energy Lett.* **2022**.
[71] R. Azmi, N. Nurrosyid, S.-H. Lee, M. Al Mubarok, W. Lee, S. Hwang, W. Yin, T. K. Ahn, T.-W. Kim, Du. Y Ryu, Y. R. Do, S.-Y. Jang, *ACS Energy Lett.* **2020**, *5*, 1396.
[72] M. A. Mahmud, H. T. Pham, T. Duong, Y. Yin, J. Peng, Y. Wu, W. Liang, L. Li, A. Kumar, H. Shen, D. Walter, H. T. Nguyen, N. Mozaffari, G. D. Tabi, G. Andersson, K. R. Catchpole, K. J. Weber, T. P. White, *Adv. Funct. Mater.* **2021**, *31*, 2104251.
[73] M. I. Saidaminov, J. Kim, A. Jain, R. Quintero-Bermudez, H. Tan, G. Long, F. Tan, A. Johnston, Y. Zhao, O. Voznyy, E. H. Sargent, *Nat. Energy* **2018**, *3*, 648.
[74] J. Chae, Q. Dong, J. Huang, A. Centrone, *Nano Lett.* **2015**, *15*, 8114.
[75] X. Liu, *Adv. Energy Mater. n/a*, 2001958.
[76] S. Jiang, R. Wang, M. Li, R. Yu, F. Wang, Z. A. Tan, *Energy Environ. Sci.* **2024**, *17*, 219.
[77] S. S. Mali, J. V. Patil, J. A. Steele, M. K. Nazeeruddin, J. H. Kim, C. K. Hong, *Energy Environ. Sci.* **2024**, *17*, 1046.
[78] F. Hermerschmidt, A. Savva, E. Georgiou, S. M. Tuladhar, J. R. Durrant, I. McCulloch, D. D. C. Bradley, C. J. Brabec, J. Nelson, S. A. Choulis, *ACS Appl. Mater. Interfaces* **2017**, *9*, 14136.